

# Masked Autoencoders as Image Processors

Huiyu Duan<sup>1,2</sup>, Wei Shen<sup>2</sup>, Xiongkuo Min<sup>1</sup>, Danyang Tu<sup>1,2</sup>, Long Teng<sup>1,2</sup>, Jia Wang<sup>1</sup>, Guangtao Zhai<sup>1,2</sup>

<sup>1</sup>Institute of Image Communication and Network Engineering, Shanghai Jiao Tong University

<sup>2</sup>MoE Key Lab of Artificial Intelligence, AI Institute, Shanghai Jiao Tong University

{huiyuduan, wei.shen, minxiongkuo, danyangtu, tenglong, jiawang, zhaiguangtao}@sjtu.edu.cn

## Abstract

Transformers have shown significant effectiveness for various vision tasks including both high-level vision and low-level vision. Recently, masked autoencoders (MAE) for feature pre-training have further unleashed the potential of Transformers, leading to state-of-the-art performances on various high-level vision tasks. However, the significance of MAE pre-training on low-level vision tasks has not been sufficiently explored. In this paper, we show that masked autoencoders are also scalable self-supervised learners for image processing tasks. We first present an efficient Transformer model considering both channel attention and shifted-window-based self-attention termed CSformer. Then we develop an effective MAE architecture for image processing (MAEIP) tasks. Extensive experimental results show that with the help of MAEIP pre-training, our proposed CSformer achieves state-of-the-art performance on various image processing tasks, including Gaussian denoising, real image denoising, single-image motion deblurring, defocus deblurring, and image deraining. The code and models will be available at: [https://github.com/DuanHuiyu/MAEIP\\_CSformer](https://github.com/DuanHuiyu/MAEIP_CSformer).

## 1. Introduction

Image processing, including image restoration, image enhancement, *etc.* has long been an important computer vision task, which aims at improving the image quality of a degraded input. A good image processor can not only produce images that are more conformed to human visual preferences, but also improve the performance of downstream computer vision tasks such as recognition, detection, segmentation, *etc* [36]. Due to the ill-posed nature of this problem, it generally requires strong image priors for effective processing. Recently, deep learning has been widely employed to image processing tasks, such as deraining, deblurring, denoising, enhancement, *etc.*, and has achieved leading performance due to its strong ability to learn generalizable priors from large-scale data [78, 13, 92].

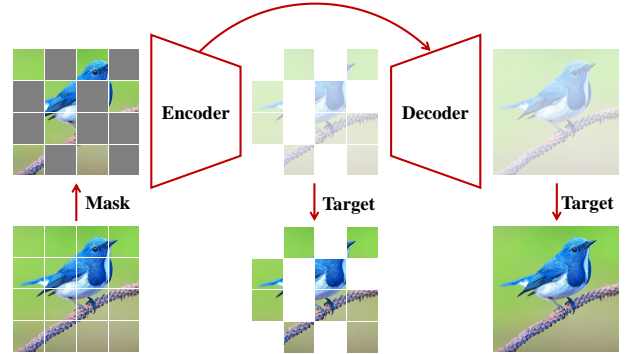


Figure 1. An illustration of the proposed MAEIP framework. The encoder predicts the raw pixel values of the randomly masked patches while the decoder predicts the raw pixel values of the whole image.

Convolutional neural networks (CNNs) have been adopted in various low-level vision tasks for many years [103, 104, 56, 109, 65, 36, 23], and have achieved impressive results. However, CNNs generally suffer from the limitation of capturing long-range pixel dependencies. Recent studies on Vision Transformers (ViT) [9, 22, 51] have explored their potential as alternatives to CNNs considering their effectiveness in capturing long-range dependencies. Some studies have also explored to use Transformers in low-level vision tasks [13, 47, 83, 92, 77], and also demonstrated the superiority of the architecture.

Besides the improvement of architectural design, recent self-supervised learning frameworks, such as DINO [10], MOCO-V3 [17], MAE [29], have further unleashed the potential of ViT and achieved high performance on various high-level vision tasks [32, 30]. Among them, masked autoencoders (MAE) [7, 110, 29, 86, 28], which pre-train image models by predicting masked tokens from seen tokens, have demonstrated superior learning ability and scalability on various high-level vision tasks. However, few studies have generalized the self-supervised pre-training strategy to image processing tasks [13].

In this paper, we show that masked autoencoders are also scalable self-supervised learners for image processing

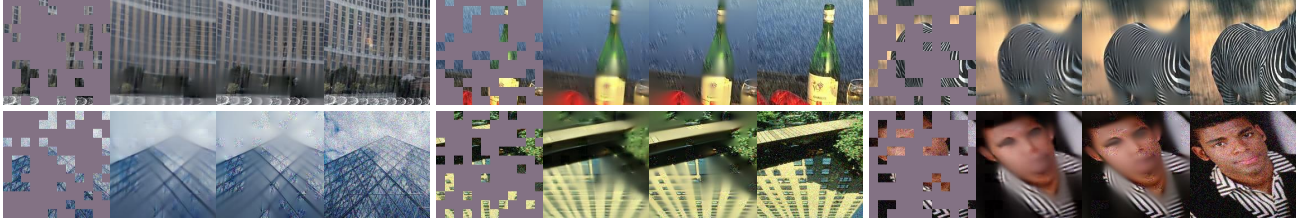


Figure 2. Example results on rainy and noisy images. For each quadruplet, we demonstrate the masked image, the reconstruction result from the encoder, the reconstruction result from the decoder, and the raw degraded image, from the left to the right, respectively.

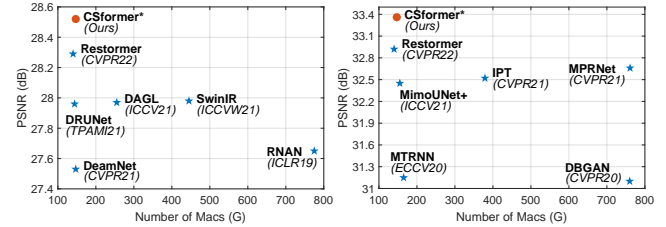
tasks. We first present an efficient Transformer for image processing. Recent studies on image processing have demonstrated the superiority of hierarchical structure [83], window-based self-attention [47], or channel-wise attention [92, 14], in terms of both performance and efficiency. Our proposed new architecture considers both channel attention and shifted-window-based self-attention and is built based on the hierarchical U-shape structure [67], which is named as CSformer. Based on the highly efficient CSformer, we further present a MAE pre-training framework for image processing (MAEIP). As shown in Figure 1, Our MAEIP masks random patches from the input image and reconstructs the masked patches and the whole image by the encoder and the decoder respectively. Similar to SIM-MIM [86], the masked input is directly fed into the encoder. Moreover, we adopt the U-shape structure [67] for high-quality whole image reconstruction.

Figure 2 gives several example results of our MAEIP framework on masked distorted images. Both the reconstruction results from the encoder and the decoder on masked pixels show that the MAE pre-training can well resist noise from the seen input and well reconstruct the expected image, which is a natural image processor. Moreover, the decoder can well keep the detailed information from the seen input, which leads to a higher-quality and more consistent reconstruction of the whole image. With the help of this effective pre-training strategy, our CSformer achieves state-of-the-art (SOTA) performance on various benchmark datasets for different image processing tasks as shown in Figure 3.

## 2. Related Work

### 2.1. Image Processing

With the development of deep learning methods and the establishment of various vision benchmarks, data-driven CNN architectures [103, 94, 95, 107, 109] have attained state-of-the-art performance on various image processing tasks compared to conventional processing approaches [19, 31, 76]. The architecture design plays an important role in improving performance, and many studies have developed general-purpose or task-specific modules for various image processing applications. Encoder-decoder-based U-Net architectures [67] have been widely adopted for image pro-



(a) Gaussian Denoising (Table 1) (b) Deblurring (Table 4)

Figure 3. PSNR results vs. computational cost.

cessing due to their high computational efficiency. Moreover, many advanced components developed for high-level vision tasks have also been introduced to low-level vision tasks and demonstrated the effectiveness, such as residual and dense connection [103, 42, 82, 109], channel attention [57, 94, 95, 23], spatial attention [81, 48, 95, 23], multi-scale or multi-stage networks [97, 41, 36, 18, 95, 15], etc.

Recently, Transformers, which are originally developed for NLP tasks [79], have been introduced to computer vision and achieved state-of-the-art performance [9, 22]. Many transformer-based architectures for high-level vision tasks have also been proposed such as ViT [22], Swin [51], PVT [80], etc. Several recent studies have also explored specific Transformer architectures for low-level vision problems. Based on DETR [9] and ViT [22], IPT [13] applies the standard Transformer encoder-decoder architecture [79] to image patches and presents a pre-training method for low-level vision tasks. However, IPT relies on large-scale datasets and multi-task learning for good performance and has huge computing complexity [47, 92]. SwinIR [47] and Uformer [83] adopt the shifted-window-based local attention module [51] in low-level tasks. However, restricting the spatial attention to local windows may also limit the long-range dependency capturing of the whole image [92]. Restormer [92] presents a multi-dconv head transposed attention (MDTA) block, which applies spatial attention across feature dimensions to reduce computational complexity. This operation can implicitly learn spatial correlation, which could be seen as a special variant of channel attention [14].

### 2.2. MAE Pre-training

Masked language modeling approaches such as BERT [38] and GPT [62, 63, 8] are successful methods for pre-

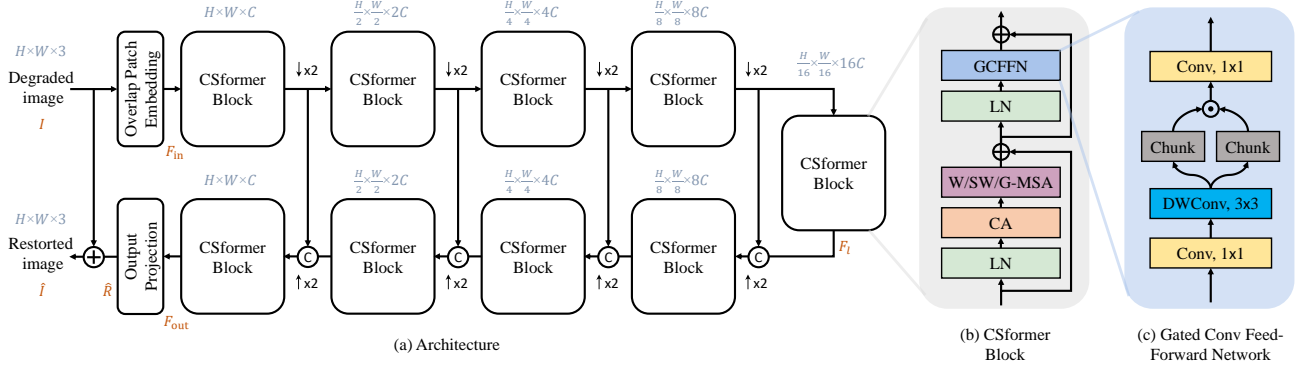


Figure 4. An overview of the proposed CSformer. (a) The architecture of the CSformer backbone. (b) An illustration of a CSformer block. (c) An illustration of the Gated Conv Feed-Forward Network (GCFFN). LN indicates a LayerNorm layer. CA is a channel-attention layer. W/SW/G-MSA represent multi-head self-attention within the regular window, shifted window, and global image, respectively.

training NLP models. Recently, some works have also explored the masking strategy in pre-training image models. iGPT [16] considers image pixels as sequences and predicts unknown pixels. BEiT [7] and iBOT [110] propose to predict discrete tokens rather than pixels to pre-train image models. MAE [29] finds that masking a high proportion of the input image can contribute to meaningful self-supervised learning, and proposes an asymmetric encoder-decoder structure to reduce pre-training time. SimMIM [86] and ConvMAE [28] propose general masked image modeling methods for hierarchical models such as Swin Transformer [51] and hybrid convolution-transformer [28]. These pre-training methods are designed for high-level vision tasks, while few studies explore self-supervised pre-training methods for low-level vision applications.

### 3. Approach

In this section, we first introduce the detailed architecture of the proposed CSformer, then we provide the details of our framework of masked autoencoders for image processing (MAEIP).

#### 3.1. CSformer

**Overall pipeline.** Figure 4-(a) demonstrates the architecture of the CSformer backbone. Our CSformer follows the design principles of encoder-decoder with skip connections, which is originally proposed by UNet [67]. Given an input degraded image  $I \in \mathbb{R}^{H \times W \times 3}$ , CSformer first applies a  $3 \times 3$  convolutional layer to extract low-level feature embeddings  $F_{in} \in \mathbb{R}^{H \times W \times C}$ . Next, these shallow feature maps  $F_{in}$  are passed through a 5-level symmetric encoder-decoder network, then output feature maps  $F_{out} \in \mathbb{R}^{H \times W \times C}$ . Each stage of the encoder-decoder contains multiple CSformer blocks, and the bottleneck stage outputs latent features  $F_l \in \mathbb{R}^{\frac{H}{16} \times \frac{W}{16} \times 16C}$ . The specific feature dimensions of each stage are shown in Figure 4-(a). We apply pixel-unshuffle and pixel-shuffle [71] for the down-sampling process in the encoder and the up-sampling process in the decoder, respectively. Similar to UNet [67], we

add skip connections between the corresponding stages of the encoder and decoder, and first concatenate two feature maps then process the concatenated features with a  $1 \times 1$  convolution to reduce the channel dimension. The output feature maps  $F_{out}$  from the encoder-decoder network are finally refined with a  $3 \times 3$  convolutional layer to get the estimated residual map  $\hat{R} \in \mathbb{R}^{H \times W \times 3}$ . The final restored image is obtained by  $\hat{I} = I + \hat{R}$ . We optimize the CSformer using the Charbonnier loss [12, 47]:  $\mathcal{L} = \sqrt{(\|\hat{I} - I'\|^2 + \varepsilon^2)}$ , where  $I'$  is the ground-truth image, and  $\varepsilon = 10^{-3}$  is a constant.

**CSformer block.** Applying self-attention among global image pixels can lead to huge computational costs [16, 51, 13]. However, image processing problems need to consider both local context information and global context information [47, 83, 92], while high-level vision transformers such as ViT show limitations in capturing local pixel dependencies [46, 83]. As shown in Figure 4-(b), similar to the standard transformer architecture [79, 22], a CSformer block consists of two parts with skip connections including an attention component and a feed-forward part. The attention component contains a channel-attention (CA) module and a window-based/shifted-window-based/global multi-head self-attention (W/SW/G-MSA) with applying a LayerNorm (LN) layer before. We apply W/SW/G-MSA across different stages. Specifically, for the bottleneck stage, whose channel-dimension is  $16C$ , we apply the global MSA to aggregate global context information, while for other stages, of which the channel-dimensions are from  $C$  to  $8C$ , we alternately apply W-MSA and SW-MSA respectively, which is similar to [51]. We adopt the gated convolutional feed-forward network (GCFFN) [20, 68, 92] as the feed-forward component with a LN layer before.

**Channel-attention.** We adopt a simplified channel-attention module [14] rather than the raw squeeze-and-excitation (SE) module [33]. Given an input tensor  $X$ , the output of the CA layer can be formulated as:  $CA(X) = X * MLP(\text{Avg}(X))$ , where Avg is an average pooling layer,

MLP is a multilayer perceptron,  $*$  indicates a channel-wise product operation. Before the channel-attention layer, a simple gate network [20, 68, 14] is also applied to control which complementary features should be adopted.

**Gated convolutional feed-forward network.** Conventional FFN [79, 46] adopts two multilayer perceptrons (MLPs) to first expand then reduce the channel dimensions to refine features. Some studies on low-level vision have manifested that adopting a lightweight depth-wise convolution in FFN can effectively enhance the locality and further improve the output quality [83, 92]. As shown in Figure 4-(c), our CSformer adopts a gated convolutional feed-forward network (GCFFN) [20, 68, 92]. Give an input tensor  $\mathbf{X}$ , the GCFFN process can be formulated as:  $\mathbf{X}_1 = W_d^1(W_p^1(\mathbf{X}))$ ,  $\mathbf{X}_2 = W_d^2(W_p^2(\mathbf{X}))$ ,  $\hat{\mathbf{X}} = W_p^3(\phi(\mathbf{X}_1) \odot \mathbf{X}_2)$ , where  $W_p$  represents a  $1 \times 1$  point-wise convolution,  $W_d$  indicates a  $3 \times 3$  depth-wise convolution,  $\phi$  is the GELU operation,  $\odot$  denotes element-wise multiplication.

**Inference process speed-up.** The Swin structure [51] is hard to test on arbitrary input size due to the hierarchical window limitation. Previous works generally need to pad the input image to a larger size as a new input, then feed it into the network [83]. This padding strategy can cause huge extra computational overhead. For instance, the window size in Uformer [83] is set to 8, which means the bottleneck layer needs to be padded to a multiple of 8. Since there are five hierarchical stages in Uformer, the input needs to be padded to a multiple of 128 during the inference process. We propose to pad the feature rather than pad the input to save extra computational overhead. Specifically, for each layer, we pad its size to the multiple of 8 and use a mask to prevent the attention calculation on the padded area. Given an extreme example, for a  $16 \times 16$  image, the spatial dimensions of the hierarchical stages in Uformer are  $128 \times 128$ ,  $64 \times 64$ ,  $32 \times 32$ ,  $16 \times 16$ ,  $8 \times 8$ , respectively, while in our CSformer are  $16 \times 16$ ,  $8 \times 8$ ,  $8 \times 8$ ,  $8 \times 8$ ,  $1 \times 1$  (this layer is not a window-based layer), respectively.

### 3.2. MAEIP

Similar to MAE [29] and SIMMIM [86], our MAEIP is a simple autoencoding approach, which masks a portion of image signals and learns to reconstruct them. We implement the MAEIP pre-training based on the CSformer. We expect that the encoder can learn more meaningful image representations, while the decoder can exploit the image representations from the encoder and the low-level details from the skip connections to reconstruct higher-quality images. Figure 1 illustrates the idea and detailed methods are introduced as follows.

**Masking.** Masked autoencoders such as BEiT [7], MAE [29], and SimMIM [86], first embed image patches to tokens, and then adopt a random mask on input tokens.

However, the same strategy cannot be directly used in our MAEIP, since low-level vision transformers including our CSformer generally adopt the overlap patch embedding strategy. Therefore, in our MAEIP, we directly mask random image patches on raw image pixels. Then the masked image is fed into the autoencoder to learn to reconstruct the original image. We follow the conventions in [29, 86] and mask random patches with  $16 \times 16$  pixels, and adopt a high masking ratio *i.e.*, 75%.

**MAEIP encoder.** The encoder in CSformer is defined as from the masked input image  $\mathbf{I}$  to the output of the bottleneck stage, *i.e.*,  $\mathbf{F}_l$ . Just as the normal training process of CSformer, the encoder directly embeds the masked images with a  $3 \times 3$  convolutional layer, and then processes the overlap embedding via a series of hierarchical CSformer blocks to get the latent features  $\mathbf{F}_l$ . The encoder reconstructs the masked input by predicting the pixel values for each masked patch. Specifically, we apply a linear layer to project the latent features  $\mathbf{F}_l$  to patch pixels [86], and compute the mean squared error (MSE) between the reconstructed and original images on the masked pixels [29].

**MAEIP decoder.** The decoder in CSformer is defined as the process from  $\mathbf{F}_l$  to the reconstructed image  $\hat{\mathbf{I}}$ . As shown in Figure 2, the reconstructed results from the encoder can only keep high-level image representations while losing image details, and may exist block artifacts between the masked area and seen area. To reconstruct higher-quality images and keep image details for facilitating subsequent image processing tasks, the MAEIP decoder learns to reconstruct the whole image. We remove the skip connection between  $\mathbf{I}$  and  $\hat{\mathbf{I}}$  in CSformer during the MAEIP pre-training, which may affect the optimization target. The decoder reconstructs the whole image by directly calculating the MSE loss between the reconstructed image  $\hat{\mathbf{I}}$  and the original image  $\mathbf{I}$  on all pixels.

**Two-stage pre-training.** Since our CSformer is a symmetric encoder-decoder network, pre-training the whole network may introduce huge computational overhead. Learning image representation is a more difficult task [29]. Therefore, we propose to pre-train MAEIP using a two-stage paradigm. In the first stage, we discard the decoder and only pre-train the MAEIP encoder. For the second stage, we apply the pre-trained encoder weights and pre-train the whole autoencoder. Experiments in Sec. 4.3 demonstrate this two-stage pre-training scheme achieves similar performance compared with the one-stage pre-training while saving pre-training time.

## 4. Experiments

We conduct extensive experiments to validate the effectiveness of the proposed model and the MAEIP pre-training framework. We evaluate the proposed approach on a wide range of different tasks, including denoising, deblurring,



Table 1. **Grayscale image denoising** results of different models. Top super row (blind denoising): learning a single model and testing on various noise levels. Bottom super row (non-blind denoising): training a separate model for each noise level.

Method	Set12 [103]			BSD68 [54]			Urban100 [34]		
	$\sigma=15$	$\sigma=25$	$\sigma=50$	$\sigma=15$	$\sigma=25$	$\sigma=50$	$\sigma=15$	$\sigma=25$	$\sigma=50$
DnCNN [103]	32.67	30.35	27.18	31.62	29.16	26.23	32.28	29.80	26.35
FFDNet [105]	32.75	30.43	27.32	31.63	29.19	26.29	32.40	29.90	26.50
IRCNN [104]	32.76	30.37	27.12	31.63	29.15	26.19	32.46	29.80	26.22
DRUNet [101]	33.25	30.94	27.90	<u>31.91</u>	<u>29.48</u>	26.59	33.44	31.11	27.96
Restormer [92]	33.35	31.04	28.01	<b>31.95</b>	<b>29.51</b>	<b>26.62</b>	33.67	31.39	28.33
CSformer*	<b>33.40</b>	<b>31.09</b>	<b>28.06</b>	<b>31.95</b>	<b>29.51</b>	<b>26.60</b>	<b>33.74</b>	<b>31.51</b>	<b>28.49</b>
<hr/>									
FOCNet [35]	33.07	30.73	27.68	31.83	29.38	26.50	33.15	30.64	27.40
MWCNN [50]	33.15	30.79	27.74	31.86	29.41	26.53	33.17	30.66	27.42
NLRN [49]	33.16	30.80	27.64	31.88	29.41	26.47	33.45	30.94	27.49
RNAN [108]	-	-	27.70	-	-	26.48	-	-	27.65
DeamNet [64]	33.19	30.81	27.74	31.91	29.44	26.54	33.37	30.85	27.53
DAGL [55]	33.28	30.93	27.81	31.93	29.46	26.51	33.79	31.39	27.97
SwinIR [47]	33.36	31.01	27.91	<b>31.97</b>	<b>29.50</b>	26.58	33.70	31.30	27.98
Restormer [92]	<u>33.42</u>	<u>31.08</u>	<u>28.00</u>	<u>31.96</u>	<b>29.52</b>	<b>26.62</b>	<u>33.79</u>	<u>31.46</u>	<u>28.29</u>
CSformer*	<b>33.44</b>	<b>31.10</b>	<b>28.08</b>	<b>31.97</b>	<b>29.52</b>	<b>26.60</b>	<b>33.83</b>	<b>31.52</b>	<b>28.52</b>

Table 2. **Color image denoising** results of different models. Our CSformer\* demonstrates great performance for both blind and non-blind denoising. On Urban dataset [34] with a noise level of 50, our CSformer\* achieves 0.15 dB gain and 0.17 dB gain compared to Restormer [92] for blind condition and non-blind condition, respectively.

Method	CBSD68 [54]			Kodak24 [24]			McMaster [106]			Urban100 [34]		
	$\sigma=15$	$\sigma=25$	$\sigma=50$	$\sigma=15$	$\sigma=25$	$\sigma=50$	$\sigma=15$	$\sigma=25$	$\sigma=50$	$\sigma=15$	$\sigma=25$	$\sigma=50$
IRCNN [104]	33.86	31.16	27.86	34.69	32.18	28.93	34.58	32.18	28.91	33.78	31.20	27.70
FFDNet [105]	33.87	31.21	27.96	34.63	32.13	28.98	34.66	32.35	29.18	33.83	31.40	28.05
DnCNN [103]	33.90	31.24	27.95	34.60	32.14	28.95	33.45	31.52	28.62	32.98	30.81	27.59
DSNet [59]	33.91	31.28	28.05	34.63	32.16	29.05	34.67	32.40	29.28	-	-	-
DRUNet [101]	34.30	31.69	<u>28.51</u>	35.31	32.89	29.86	35.40	33.14	30.08	34.81	32.60	29.61
Restormer [92]	<u>34.39</u>	<u>31.78</u>	<b>28.59</b>	<u>35.44</u>	<u>33.02</u>	<u>30.00</u>	<u>35.55</u>	<u>33.31</u>	<u>30.29</u>	<u>35.06</u>	<u>32.91</u>	<u>30.02</u>
CSformer*	<b>34.40</b>	<b>31.79</b>	<b>28.59</b>	<b>35.48</b>	<b>33.06</b>	<b>30.04</b>	<b>35.59</b>	<b>33.36</b>	<b>30.33</b>	<b>35.13</b>	<b>33.02</b>	<b>30.17</b>
<hr/>												
RPCNN [85]	-	31.24	28.06	-	32.34	29.25	-	32.33	29.33	-	31.81	28.62
BRDNet [75]	34.10	31.43	28.16	34.88	32.41	29.22	35.08	32.75	29.52	34.42	31.99	28.56
RNAN [108]	-	-	28.27	-	-	29.58	-	-	29.72	-	-	29.08
RDN [109]	-	-	28.31	-	-	29.66	-	-	-	-	-	29.38
IPT [13]	-	-	28.39	-	-	29.64	-	-	29.98	-	-	29.71
SwinIR [47]	<b>34.42</b>	31.78	<u>28.56</u>	35.34	32.89	29.79	35.61	33.20	30.22	35.13	32.90	29.82
Restormer [92]	<u>34.40</u>	<u>31.79</u>	<b>28.60</b>	<u>35.47</u>	<u>33.04</u>	<u>30.01</u>	<u>35.61</u>	<u>33.34</u>	<u>30.30</u>	<u>35.13</u>	<u>32.96</u>	<u>30.02</u>
CSformer*	<b>34.42</b>	<b>31.81</b>	<b>28.60</b>	<b>35.50</b>	<b>33.09</b>	<b>30.06</b>	<b>35.63</b>	<b>33.39</b>	<b>30.35</b>	<b>35.20</b>	<b>33.08</b>	<b>30.19</b>

Table 3. **Real image denoising** results on SIDD [1] and DND [60] datasets.

Dataset	Method	RIDNet	AINDNet	VDN	SADNet	DANet+	CycleISP	MIRNet	DeamNet	MPRNet	DAGL	Uformer	MAXIM	Restormer	CSformer	CSformer*
		[5]	[39]	[90]	[11]	[91]	[93]	[94]	[64]	[95]	[55]	[83]	[77]	[92]	(Ours)	(Ours)
SIDD [1]	PSNR $\uparrow$	38.71	39.08	39.28	39.46	39.47	39.52	39.72	39.47	39.71	38.94	39.89	39.96	<u>40.02</u>	40.00	<b>40.05</b>
	SSIM $\uparrow$	0.951	0.954	0.956	0.957	0.957	0.957	0.959	0.957	0.958	0.953	0.960	0.960	<u>0.960</u>	<u>0.960</u>	<b>0.961</b>
DND [60]	PSNR $\uparrow$	39.26	39.37	39.38	39.59	39.58	39.56	39.88	39.63	39.80	39.77	39.98	39.84	<b>40.03</b>	40.00	<u>40.02</u>
	SSIM $\uparrow$	0.953	0.951	0.952	0.952	0.955	0.956	0.956	0.953	0.954	0.956	0.955	0.954	<b>0.956</b>	<b>0.956</b>	<b>0.956</b>

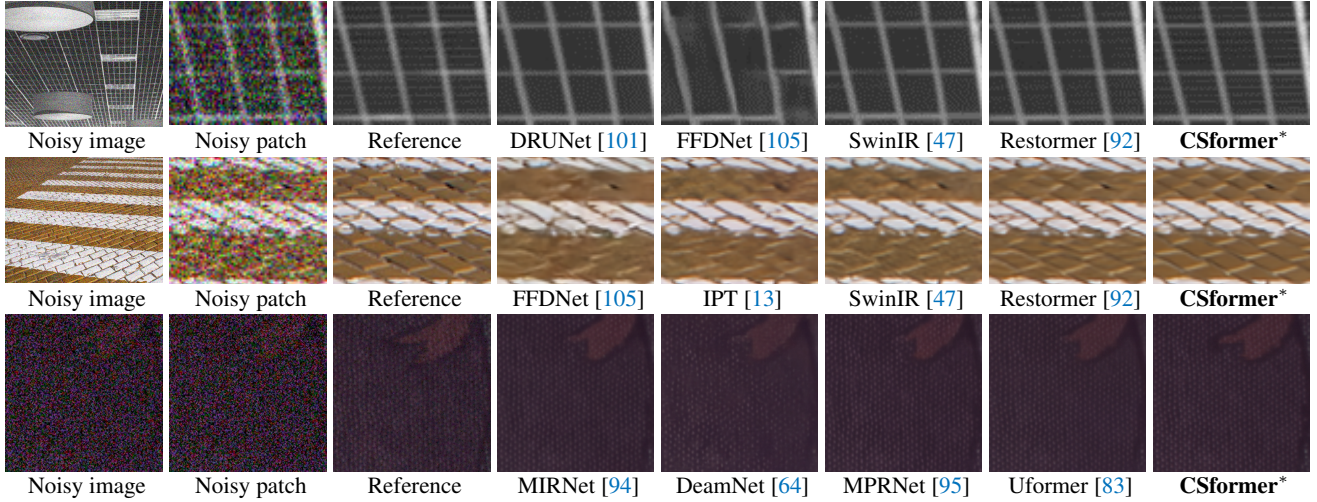


Figure 5. **Image denoising** visualization comparisons. Top row: grayscale Gaussian noise removal on Urban100 [34] ( $\sigma = 50$ ). Middle row: color image Gaussian noise removal on Urban100 [34] ( $\sigma = 50$ ). Bottom row: real image denoising on SIDD [1].

and deraining. More experiments on other tasks such as image enhancement *etc.*, and more comprehensive results and visualizations can be found in the *supplementary material*. We **bold** the best results and underline the second-best results in the tables.

#### 4.1. Experimental Setup

**Architectural configuration.** We introduce three CSformer variants in our experiments including CSformer-T

(Tiny), CSformer-T2, and CSformer by setting different base feature channels  $C$  and the number of CSformer blocks in each encoder and decoder stage. The design of the encoder and decoder in CSformer adopts a symmetrical structure. The detailed architecture for each variant is listed in the supplementary material.

**Training details.** Our proposed CSformer is end-to-end trainable without pre-training [13] or progressive training [36, 92]. However, with the help of self-supervised MAEIP

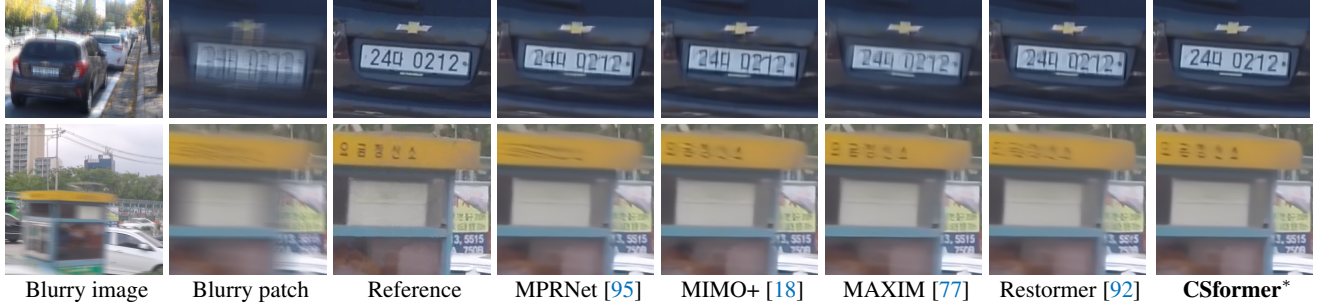


Figure 6. **Motion deblurring** results on GoPro [56] test set. Our CSformer\* effectively removes blur and generates more faithful results.

Table 4. **Motion deblurring** results. Our CSformer\* is only trained on the GoPro training set [56], and directly evaluated on the GoPro test set [56], HIDE [69], and RealBlur-R&J [66]

Method	GoPro [56]		HIDE [69]		RealBlur-R [66]		RealBlur-J [66]	
	PSNR	SSIM	PSNR	SSIM	PSNR	SSIM	PSNR	SSIM
Xu <i>et al.</i> [87]	21.00	0.741	-	-	34.46	0.937	27.14	0.830
DeblurGAN [40]	28.70	0.858	24.51	0.871	33.79	0.903	27.97	0.834
Nah <i>et al.</i> [56]	29.08	0.914	25.73	0.874	32.51	0.841	27.87	0.827
Zhang <i>et al.</i> [100]	29.19	0.931	-	-	35.48	0.947	27.80	0.847
DeblurGAN-v2 [41]	29.55	0.934	26.61	0.875	35.26	0.944	28.70	0.866
SRN [74]	30.26	0.934	28.36	0.915	35.66	0.947	28.56	0.867
Shen <i>et al.</i> [69]	-	-	28.89	0.930	-	-	-	-
Gao <i>et al.</i> [27]	30.90	0.935	29.11	0.913	-	-	-	-
DBGAN [102]	31.10	0.942	28.94	0.915	33.78	0.909	24.93	0.745
MT-RNN [58]	31.15	0.945	29.15	0.918	35.79	0.951	28.44	0.862
DMPHN [97]	31.20	0.940	29.09	0.924	35.70	0.948	28.42	0.860
Suin <i>et al.</i> [73]	31.85	0.948	29.98	0.930	-	-	-	-
SPAIR [61]	32.06	0.953	30.29	0.931	-	-	<u>28.81</u>	<u>0.875</u>
MIMO-UNet+ [18]	32.45	0.957	29.99	0.930	35.54	0.947	27.63	0.837
IPT [13]	32.52	-	-	-	-	-	-	-
MPRNet [95]	32.66	0.959	30.96	0.939	35.99	0.952	28.70	0.873
Restormer [92]	<u>32.92</u>	<u>0.961</u>	<u>31.22</u>	<u>0.942</u>	<u>36.19</u>	<u>0.957</u>	<b>28.96</b>	<b>0.879</b>
<b>CSformer*</b>	<b>33.36</b>	<b>0.965</b>	<b>31.39</b>	<b>0.945</b>	<b>36.29</b>	<b>0.958</b>	<u>28.81</u>	0.873

pre-training, the performance can be further improved. In the following experiments, we use \* to indicate a CSformer that has been pre-trained with MAEIP before finetuning, *i.e.*, CSformer\*. We perform self-supervised pre-training on the ImageNet-1K (IN1K) [21] training set with  $192 \times 192$  random-cropped patches. Due to the limitation of computing resources, we only pre-train MAEIP for 100 epochs on IN1K. For two-stage pre-training, we first pre-train the encoder for 50 epochs and then pre-train the whole network for 50 epochs. After MAEIP pre-training, we finetune separate models for different image processing tasks. Generally, the CSformer is trained on  $192 \times 192$  random-cropped patches with random data augmentation methods including horizontal and vertical flips,  $90^\circ$  rotations, and MixUp [96]. For the tasks that highly depend on long-range dependencies and usually have high-resolution inputs, *i.e.*, motion deblurring and defocus deblurring, the CSformer is finetuned on  $256 \times 256$  random-cropped patches. We generally train CSformer using the AdamW optimizer for 600K iterations with an initial learning rate of  $2e^{-4}$ , and gradually reduce the learning rate to  $1e^{-6}$  with the cosine annealing [52].

Without specific instructions, we test the CSformer on full-resolution images rather than on small patches.

## 4.2. Benchmark Results

**Gaussian denoising.** We first conduct denoising experiments on synthetic datasets with additive white Gaussian noise. Following previous conventions [103, 47, 92], we train the gaussian denoising model on four datasets including DIV2K [4], Flickr2K, BSD500 [6], WaterlooED [53], and test on five datasets including Set12 [103], BSD68 [54], Urban100 [34], Kodak24 [24], and McMaster [106]. We consider three noise levels including 15, 25, and 50. We conduct two types of gaussian denoising experiments, including learning a single denoising model to deal with various noise levels (blind denoising) and learning separate models for different noise levels respectively (non-blind denoising). Table 1 and Table 2 show PSNR results of different models for grayscale image denoising and color image denoising, respectively. Our CSformer\* achieves state-of-the-art performance compared to other models. Specifically, on the grayscale Urban100 [34] dataset with a noise level of 50, CSformer\* yields 0.23 dB gain over Restormer [92] and 0.54 dB gain over SwinIR [47], respectively, for the non-blind denoising task. The top row and middle row in Figure 5 show visualization results of different denoising models. Our CSformer\* produces images that are more conformed to human visual preference.

**Real denoising.** We further conduct denoising experiments on real-world datasets, *i.e.*, SIDD [1] and DND [60]. Following the previous conventions [83, 77, 92], we only train CSformer on the SIDD [1] training set and directly test on the SIDD [1] and DND [60] test sets. Quantitative results in Table 3 demonstrate that our CSformer\* achieves state-of-the-art performance on the SIDD dataset and obtains competitive performance on the DND dataset. Moreover, without MAEIP pre-training, our CSformer still outperforms most of the SOTA models, which also manifests the superiority of the CSformer. The bottom row in Figure 5 also qualitatively demonstrates the effectiveness of our CSformer\* on real denoising.

**Motion deblurring.** Following previous experimental set-

Table 5. **Defocus deblurring** comparisons of the state-of-the-art models on the DPDD test set [2], which contains 37 indoor scenes and 39 outdoor scenes. **S**: single-image defocus deblurring. **D**: dual-pixel defocus deblurring.

Method	Indoor Scenes				Outdoor Scenes				Combined			
	PSNR $\uparrow$	SSIM $\uparrow$	MAE $\downarrow$	LPIPS $\downarrow$	PSNR $\uparrow$	SSIM $\uparrow$	MAE $\downarrow$	LPIPS $\downarrow$	PSNR $\uparrow$	SSIM $\uparrow$	MAE $\downarrow$	LPIPS $\downarrow$
EBDB <sub>S</sub> [37]	25.77	0.772	0.040	0.297	21.25	0.599	0.058	0.373	23.45	0.683	0.049	0.336
DMENet <sub>S</sub> [43]	25.50	0.788	0.038	0.298	21.43	0.644	0.063	0.397	23.41	0.714	0.051	0.349
JNB <sub>S</sub> [70]	26.73	0.828	0.031	0.273	21.10	0.608	0.064	0.355	23.84	0.715	0.048	0.315
DPDNet <sub>S</sub> [2]	26.54	0.816	0.031	0.239	22.25	0.682	0.056	0.313	24.34	0.747	0.044	0.277
KPAC <sub>S</sub> [72]	27.97	0.852	0.026	0.182	22.62	0.701	0.053	0.269	25.22	0.774	0.040	0.227
IFAN <sub>S</sub> [44]	28.11	0.861	0.026	0.179	22.76	0.720	0.052	0.254	25.37	0.789	0.039	0.217
Restormer <sub>S</sub> [92]	<u>28.87</u>	<u>0.882</u>	<u>0.025</u>	<u>0.145</u>	<u>23.24</u>	<u>0.743</u>	<u>0.050</u>	<u>0.209</u>	<u>25.98</u>	<u>0.811</u>	<u>0.038</u>	<u>0.178</u>
<b>CSformer<sub>S</sub>*</b>	<b>29.01</b>	<b>0.883</b>	<b>0.023</b>	<b>0.139</b>	<b>23.63</b>	<b>0.759</b>	<b>0.047</b>	<b>0.191</b>	<b>26.25</b>	<b>0.819</b>	<b>0.036</b>	<b>0.166</b>
DPDNet <sub>D</sub> [2]	27.48	0.849	0.029	0.189	22.90	0.726	0.052	0.255	25.13	0.786	0.041	0.223
RDPD <sub>D</sub> [3]	28.10	0.843	0.027	0.210	22.82	0.704	0.053	0.298	25.39	0.772	0.040	0.255
Uformer <sub>D</sub> [83]	28.23	0.860	0.026	0.199	23.10	0.728	0.051	0.285	25.65	0.795	0.039	0.243
IFAN <sub>D</sub> [44]	28.66	0.868	<u>0.025</u>	0.172	23.46	0.743	0.049	0.240	25.99	0.804	0.037	<u>0.207</u>
Restormer <sub>D</sub> [92]	<u>29.48</u>	<u>0.895</u>	<b>0.023</b>	<u>0.134</u>	<u>23.97</u>	<u>0.773</u>	<u>0.047</u>	<b>0.175</b>	<u>26.66</u>	<u>0.833</u>	<u>0.035</u>	<b>0.155</b>
<b>CSformer<sub>D</sub>*</b>	<b>29.54</b>	<b>0.896</b>	<b>0.023</b>	<b>0.130</b>	<b>24.38</b>	<b>0.788</b>	<b>0.045</b>	<u>0.179</u>	<b>26.89</b>	<b>0.841</b>	<b>0.034</b>	<b>0.155</b>

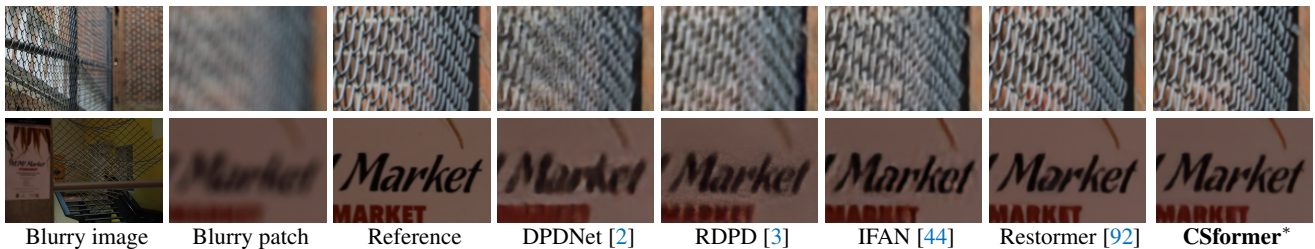


Figure 7. **Defocus deblurring** results on the DPDD [2] test set. Our CSformer\* effectively removes blur and generates sharper results.

tings on motion deblurring [95, 83, 92], we only train CSformer\* on the GoPro [56] training set and directly test the performance on four test sets, including two synthetic datasets (GoPro test set [56], HIDE [69]) and two real-world datasets (RealBlur-R [66], RealBlur-J [66]). The CSformer\* is tested on full-resolution images rather than on patches [14]. Table 4 shows the quantitative comparisons of different models on the four test sets. Our CSformer\* achieves a performance boost of 0.44 dB over the Restormer [92] on the GoPro test set. Moreover, our CSformer\* also generalizes well on the other three test sets. Figure 6 demonstrates the visualization results of different deblurring models. It can be observed that our CSformer\* generates more visually-faithful results compared to other methods.

**Defocus deblurring.** We conduct the defocus deblurring experiments on the DPDD dataset [2]. We consider two cases including the single-image defocus deblurring and the dual-pixel defocus deblurring. For dual-pixel defocus deblurring, we directly concatenate the left image and the right image in the channel dimension, and then input it to the CSformer\*. Table 5 shows the quantitative comparisons of state-of-the-art models on the DPDD test set. Our CSformer\* outperforms previous models on almost all evaluation criteria for both tasks and both scenes. Figure 7 illustrates that our method is more effective in removing defocus blur compared to other approaches.

**Deraining.** Following previous works [36, 95, 77], for single image deraining experiments, we train CSformer\* on a comprehensive training set [36], and test the performance on five test sets including Rain100L [88], Rain100H [88], Test100 [99], Test1200 [98], and Test 2800 [26]. Table 6 shows quantitative comparisons with several previous methods. It can be observed that our CSformer\* achieves state-of-the-art performances on all test sets. Figure 8 also gives some examples of the visualization results of different deraining methods. Our method produces rain-free images with structural fidelity and without introducing noticeable artifacts.

### 4.3. Ablation Studies

We conduct extensive ablation experiments to validate the effectiveness of the proposed CSformer model and the MAEIP pre-training method. We first evaluate the effectiveness of the CSformer architecture on the SIDD dataset [1] using the variant CSformer-T2. We also design several pre-training variants and validate the effect of the MAEIP framework on image deraining [36] using CSformer-T.

**Improvements on CSformer architecture.** The number of blocks for each hierarchical stage in CSformer-T2 is same with the Uformer-T [83]. The second row in Table 7-A shows the performance of Uformer-T on SIDD [1] test set. By replacing the LeFF module with the GCFFN (GC) module, the performance achieves 0.02 dB gain while reducing



Table 6. Quantitative comparisons of the state-of-the-art models for **image deraining**.

Method	Rain100L [88]		Rain100H [88]		Test100 [99]		Test1200 [98]		Test2800 [26]		Average	
	PSNR↑	SSIM↑	PSNR↑	SSIM↑	PSNR↑	SSIM↑	PSNR↑	SSIM↑	PSNR↑	SSIM↑	PSNR↑	SSIM↑
DerainNet [25]	27.03	0.884	14.92	0.592	22.77	0.810	23.38	0.835	24.31	0.861	22.48	0.796
SEMI [84]	25.03	0.842	16.56	0.486	22.35	0.788	26.05	0.822	24.43	0.782	22.88	0.744
DIDMDN [98]	25.23	0.741	17.35	0.524	22.56	0.818	29.65	0.901	28.13	0.867	24.58	0.770
UMRL [89]	29.18	0.923	26.01	0.832	24.41	0.829	30.55	0.910	29.97	0.905	28.02	0.880
RESCAN [45]	29.80	0.881	26.36	0.786	25.00	0.835	30.51	0.882	31.29	0.904	28.59	0.857
PreNet [65]	32.44	0.950	26.77	0.858	24.81	0.851	31.36	0.911	31.75	0.916	29.42	0.897
MSPFN [36]	32.40	0.933	28.66	0.860	27.50	0.876	32.39	0.916	32.82	0.930	30.75	0.903
MPRNet [95]	36.40	0.965	30.41	0.890	30.27	0.897	32.91	0.916	33.64	0.938	32.73	0.921
HINet [15]	37.20	0.969	30.63	0.893	30.26	0.905	<u>33.01</u>	0.918	<u>33.87</u>	0.940	33.00	0.925
MAXIM-2S [77]	<u>38.06</u>	<u>0.977</u>	<u>30.81</u>	<u>0.903</u>	<u>31.17</u>	<u>0.922</u>	32.37	<u>0.922</u>	33.80	<u>0.943</u>	<u>33.24</u>	<u>0.933</u>
<b>CSformer*</b>	<b>39.49</b>	<b>0.978</b>	<b>32.00</b>	<b>0.912</b>	<b>32.02</b>	<b>0.925</b>	<b>33.19</b>	<b>0.925</b>	<b>33.81</b>	<b>0.943</b>	<b>34.10</b>	<b>0.937</b>

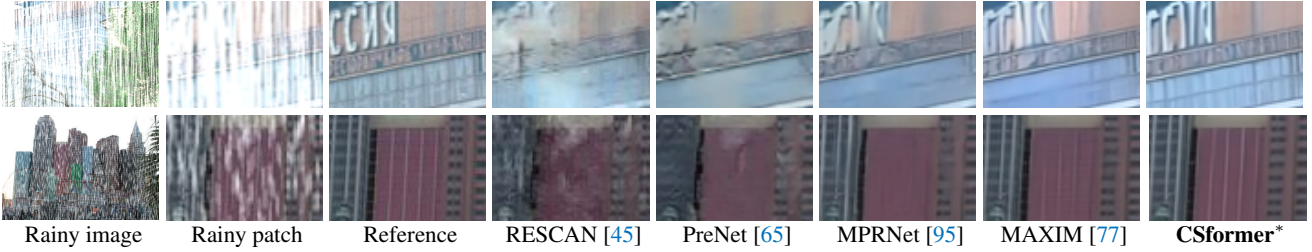
Figure 8. **Image deraining** visualization results. Our CSformer\* produces more visually pleasant rain-free results.

Table 7. Ablation studies of individual components in CSformer and the MAEIP pre-training method.

GC	Sym	GA	CA	GMACs	PSNR	Variant	Rain100L	Test100	Avg.
				12.00	39.66	w/o p.	37.03	30.53	33.78
✓				11.69	39.68	r. encoder	37.11	30.90	34.00
✓	✓			12.66	39.72	r. decoder	37.35	30.99	34.17
✓	✓	✓		12.66	39.74	MAEIP	37.48	31.07	34.28
✓	✓	✓	✓	13.50	39.77	2-stage	37.43	31.07	34.25

A. Individual components.

B. PSNRs of pre-training variants.

the computational complexity. The original Uformer-T is an asymmetric structure, of which the number of channels in the decoder is twice the number of channels in the corresponding encoder. By adjusting this asymmetric structure to the symmetric structure (Sym), in which the corresponding encoder and decoder have the same number of channels, the model further achieves a 0.04 dB gain. Moreover, by adopting the global MSA (GA) in the bottleneck stage, the performance can be further improved. Finally, we add channel-attention modules (CA) to the model and adjust the mlp ratio to achieve a similar computational complexity, which further improves the performance by 0.03 dB. Through these improvements, our CSformer-T2 achieves the same performance as Uformer-S (39.77 dB) with fewer computational costs (13.50 GMACs *vs.* 43.86 GMACs).

**Effectiveness of the MAEIP pre-training.** We consider five different pre-training variants including (1) without pre-training (w/o p.), (2) only reconstructing encoder output (r. encoder), *i.e.*, only pre-training encoder, (3) only reconstructing decoder output (r. decoder), (4) our MAEIP framework, *i.e.*, reconstructing encoder output and decoder

Table 8. PSNR results of different pre-training length.

	Rain100L [88]	Test100 [99]	Average
w/o pre-training	37.03	30.53	33.78
30 epochs	37.28	30.95	34.11
60 epochs	37.48	31.07	34.28

output simultaneously, and (5) a 2-stage pre-training. We conduct this ablation experiment based on CSformer-T, which is a more lightweight model, and pre-train these variants for 60 epochs. Table 7-B demonstrates the finetuned performance of these pre-training variants on the image deraining task. We follow the benchmark experimental settings and report the test results on the Rain100L [88] and Test100 [99] datasets. Our MAEIP pre-training boosts the performance of CSformer-T by 0.5 dB on average, which is better than only reconstructing the encoder output or only reconstructing the decoder output. For 2-stage pre-training, we first pre-train the encoder for 30 epochs, then pre-train the whole framework for 30 epochs. The 2-stage pre-training achieves similar performance but the first-stage pre-training saves about half of the training time (25% time saving overall), which is a more efficient pre-training method. Moreover, as shown in Table 3, our MAEIP framework still works well for large CSformer models.

**Influence of the pre-training length.** We also validate whether the training schedule length influences the finetuned performance. As shown in Table 8, the CSformer-T pre-trained for 30 epochs significantly performs better than without pre-training, but worse than pre-trained for 60 epochs, which shows that the performance improves steadily with longer pre-training [29].



## 5. Conclusion

This paper demonstrates that masked autoencoders are also effective self-supervised learning frameworks for image processing tasks. We first devise an efficient CSformer model, which considers both channel attention and shifted-window-based self-attention. Then we propose an effective MAE architecture for image processing tasks termed MAEIP, and implement the pre-training process based on the proposed excellent CSformer model. Extensive experiments show that the CSformer pre-trained with the self-supervised framework MAEIP achieves state-of-the-art performance on several image processing tasks, and our CSformer is also computationally efficient. We demonstrate a few applications, but our pre-trained CSformer is also expected to perform well on other tasks and applications.

## References

- [1] Abdelrahman Abdelhamed, Stephen Lin, and Michael S Brown. A high-quality denoising dataset for smartphone cameras. In *Proceedings of the IEEE Conference on Computer Vision and Pattern Recognition (CVPR)*, pages 1692–1700, 2018.
- [2] Abdullah Abuolaim and Michael S Brown. Defocus deblurring using dual-pixel data. In *Proceedings of the European Conference on Computer Vision (ECCV)*, pages 111–126, 2020.
- [3] Abdullah Abuolaim, Mauricio Delbracio, Damien Kelly, Michael S. Brown, and Peyman Milanfar. Learning to reduce defocus blur by realistically modeling dual-pixel data. In *Proceedings of the IEEE International Conference on Computer Vision (ICCV)*, pages 2289–2298, 2021.
- [4] Eirikur Agustsson and Radu Timofte. Ntire 2017 challenge on single image super-resolution: Dataset and study. In *Proceedings of the IEEE Conference on Computer Vision and Pattern Recognition Workshops (CVPRW)*, pages 126–135, 2017.
- [5] Saeed Anwar and Nick Barnes. Real image denoising with feature attention. *Proceedings of the IEEE International Conference on Computer Vision (ICCV)*, pages 3155–3164, 2019.
- [6] Pablo Arbelaez, Michael Maire, Charless Fowlkes, and Jitendra Malik. Contour detection and hierarchical image segmentation. *IEEE Transactions on Pattern Analysis and Machine Intelligence (TPAMI)*, 33(5):898–916, 2010.
- [7] Hangbo Bao, Li Dong, Songhao Piao, and Furu Wei. Bert pre-training of image transformers. In *Proceedings of the International Conference on Learning Representations (ICLR)*, 2022.
- [8] Tom Brown, Benjamin Mann, Nick Ryder, Melanie Subbiah, Jared D Kaplan, Prafulla Dhariwal, Arvind Neelakantan, Pranav Shyam, Girish Sastry, Amanda Askell, et al. Language models are few-shot learners. In *Proceedings of the Advances in Neural Information Processing Systems (NeurIPS)*, 2020.
- [9] Nicolas Carion, Francisco Massa, Gabriel Synnaeve, Nicolas Usunier, Alexander Kirillov, and Sergey Zagoruyko. End-to-end object detection with transformers. In *Proceedings of the European Conference on Computer Vision (ECCV)*, pages 213–229. Springer, 2020.
- [10] Mathilde Caron, Hugo Touvron, Ishan Misra, Hervé Jégou, Julien Mairal, Piotr Bojanowski, and Armand Joulin. Emerging properties in self-supervised vision transformers. In *Proceedings of the IEEE International Conference on Computer Vision (ICCV)*, pages 9650–9660, 2021.
- [11] Meng Chang, Qi Li, Huajun Feng, and Zhihai Xu. Spatial-adaptive network for single image denoising. In *Proceedings of the European Conference on Computer Vision (ECCV)*, pages 171–187, 2020.
- [12] Pierre Charbonnier, Laure Blanc-Feraud, Gilles Aubert, and Michel Barlaud. Two deterministic half-quadratic regularization algorithms for computed imaging. In *Proceedings of the IEEE International Conference on Image Processing (ICIP)*, volume 2, pages 168–172, 1994.
- [13] Hanting Chen, Yunhe Wang, Tianyu Guo, Chang Xu, Yiping Deng, Zhenhua Liu, Siwei Ma, Chunjing Xu, Chao Xu, and Wen Gao. Pre-trained image processing transformer. In *Proceedings of the IEEE Conference on Computer Vision and Pattern Recognition (CVPR)*, pages 12299–12310, 2021.
- [14] Liangyu Chen, Xiaojie Chu, Xiangyu Zhang, and Jian Sun. Simple baselines for image restoration. In *Proceedings of the European Conference on Computer Vision (ECCV)*, pages 17–33. Springer, 2022.
- [15] Liangyu Chen, Xin Lu, Jie Zhang, Xiaojie Chu, and Chengpeng Chen. Hinet: Half instance normalization network for image restoration. In *Proceedings of the IEEE Conference on Computer Vision and Pattern Recognition (CVPR)*, pages 182–192, 2021.
- [16] Mark Chen, Alec Radford, Rewon Child, Jeffrey Wu, Heewoo Jun, David Luan, and Ilya Sutskever. Generative pre-training from pixels. In *Proceedings of the International Conference on Machine Learning (ICML)*, pages 1691–1703, 2020.
- [17] Xinlei Chen, Saining Xie, and Kaiming He. An empirical study of training self-supervised vision transformers. In *Proceedings of the IEEE International Conference on Computer Vision (ICCV)*, pages 9640–9649, 2021.
- [18] Sung-Jin Cho, Seo-Won Ji, Jun-Pyo Hong, Seung-Won Jung, and Sung-Jea Ko. Rethinking coarse-to-fine approach in single image deblurring. In *Proceedings of the IEEE International Conference on Computer Vision (ICCV)*, pages 4641–4650, 2021.
- [19] Kostadin Dabov, Alessandro Foi, Vladimir Katkovnik, and Karen Egiazarian. Image denoising by sparse 3-D transform-domain collaborative filtering. *IEEE Transactions on Image Processing (TIP)*, 16(8):2080–2095, 2007.
- [20] Yann N Dauphin, Angela Fan, Michael Auli, and David Grangier. Language modeling with gated convolutional networks. In *Proceedings of the International Conference on Machine Learning (ICML)*, pages 933–941, 2017.
- [21] Jia Deng, Wei Dong, Richard Socher, Li-Jia Li, Kai Li, and Li Fei-Fei. Imagenet: A large-scale hierarchical image database. In *Proceedings of the IEEE Conference on*

- Computer Vision and Pattern Recognition (CVPR)*, pages 248–255, 2009.
- [22] Alexey Dosovitskiy, Lucas Beyer, Alexander Kolesnikov, Dirk Weissenborn, Xiaohua Zhai, Thomas Unterthiner, Mostafa Dehghani, Matthias Minderer, Georg Heigold, Sylvain Gelly, et al. An image is worth 16x16 words: Transformers for image recognition at scale. In *Proceedings of the International Conference on Learning Representations (ICLR)*, 2021.
  - [23] Huiyu Duan, Wei Shen, Xiongkuo Min, Yuan Tian, Jae-Hyun Jung, Xiaokang Yang, and Guangtao Zhai. Develop then rival: A human vision-inspired framework for super-imposed image decomposition. *IEEE Transactions on Multimedia (TMM)*, 2022.
  - [24] Rich Franzen. Kodak lossless true color image suite. <http://r0k.us/graphics/kodak/>, 1999. Online accessed 24 Oct 2021.
  - [25] Xueyang Fu, Jiabin Huang, Xinghao Ding, Yinghao Liao, and John Paisley. Clearing the skies: A deep network architecture for single-image rain removal. *IEEE Transactions on Image Processing (TIP)*, 26(6):2944–2956, 2017.
  - [26] Xueyang Fu, Jiabin Huang, Delu Zeng, Yue Huang, Xinghao Ding, and John Paisley. Removing rain from single images via a deep detail network. In *Proceedings of the IEEE Conference on Computer Vision and Pattern Recognition (CVPR)*, pages 3855–3863, 2017.
  - [27] Hongyun Gao, Xin Tao, Xiaoyong Shen, and Jiaya Jia. Dynamic scene deblurring with parameter selective sharing and nested skip connections. In *Proceedings of the IEEE Conference on Computer Vision and Pattern Recognition (CVPR)*, pages 3848–3856, 2019.
  - [28] Peng Gao, Teli Ma, Hongsheng Li, Jifeng Dai, and Yu Qiao. Convmc: Masked convolution meets masked autoencoders. In *Proceedings of the Advances in Neural Information Processing Systems (NeurIPS)*, 2022.
  - [29] Kaiming He, Xinlei Chen, Saining Xie, Yanghao Li, Piotr Dollár, and Ross Girshick. Masked autoencoders are scalable vision learners. In *Proceedings of the IEEE Conference on Computer Vision and Pattern Recognition (CVPR)*, pages 16000–16009, 2022.
  - [30] Kaiming He, Georgia Gkioxari, Piotr Dollár, and Ross Girshick. Mask r-cnn. In *Proceedings of the IEEE International Conference on Computer Vision (ICCV)*, pages 2961–2969, 2017.
  - [31] Kaiming He, Jian Sun, and Xiaoou Tang. Single image haze removal using dark channel prior. *IEEE Transactions on Pattern Analysis and Machine Intelligence (TPAMI)*, 33(12):2341–2353, 2010.
  - [32] Kaiming He, Xiangyu Zhang, Shaoqing Ren, and Jian Sun. Deep residual learning for image recognition. In *Proceedings of the IEEE Conference on Computer Vision and Pattern Recognition (CVPR)*, pages 770–778, 2016.
  - [33] Jie Hu, Li Shen, and Gang Sun. Squeeze-and-excitation networks. In *Proceedings of the IEEE Conference on Computer Vision and Pattern Recognition (CVPR)*, pages 7132–7141, 2018.
  - [34] Jia-Bin Huang, Abhishek Singh, and Narendra Ahuja. Single image super-resolution from transformed self-exemplars. In *Proceedings of the IEEE Conference on Computer Vision and Pattern Recognition (CVPR)*, pages 5197–5206, 2015.
  - [35] Xixi Jia, Sanyang Liu, Xiangchu Feng, and Lei Zhang. Focnet: A fractional optimal control network for image denoising. In *Proceedings of the IEEE Conference on Computer Vision and Pattern Recognition (CVPR)*, pages 6054–6063, 2019.
  - [36] Kui Jiang, Zhongyuan Wang, Peng Yi, Baojin Huang, Yimin Luo, Jiayi Ma, and Junjun Jiang. Multi-scale progressive fusion network for single image deraining. In *Proceedings of the IEEE Conference on Computer Vision and Pattern Recognition (CVPR)*, pages 8346–8355, 2020.
  - [37] Ali Karaali and Claudio Rosito Jung. Edge-based defocus blur estimation with adaptive scale selection. *IEEE Transactions on Image Processing (TIP)*, 27(3):1126–1137, 2017.
  - [38] Jacob Devlin Ming-Wei Chang Kenton and Lee Kristina Toutanova. Bert: Pre-training of deep bidirectional transformers for language understanding. In *Proceedings of NAACL*, pages 4171–4186, 2019.
  - [39] Yoonsik Kim, Jae Woong Soh, Gu Yong Park, and Nam Ik Cho. Transfer learning from synthetic to real-noise denoising with adaptive instance normalization. In *Proceedings of the IEEE Conference on Computer Vision and Pattern Recognition (CVPR)*, pages 3482–3492, 2020.
  - [40] Orest Kupyn, Volodymyr Budzan, Mykola Mykhailych, Dmytro Mishkin, and Jiří Matas. DeblurGAN: Blind motion deblurring using conditional adversarial networks. In *Proceedings of the IEEE Conference on Computer Vision and Pattern Recognition (CVPR)*, pages 8183–8192, 2018.
  - [41] Orest Kupyn, Tetiana Martyniuk, Junru Wu, and Zhangyang Wang. DeblurGAN-v2: Deblurring (orders-of-magnitude) faster and better. In *Proceedings of the IEEE International Conference on Computer Vision (ICCV)*, pages 8878–8887, 2019.
  - [42] Christian Ledig, Lucas Theis, Ferenc Huszár, Jose Caballero, Andrew Cunningham, Alejandro Acosta, Andrew Aitken, Alykhan Tejani, Johannes Totz, Zehan Wang, et al. Photo-realistic single image super-resolution using a generative adversarial network. In *Proceedings of the IEEE Conference on Computer Vision and Pattern Recognition (CVPR)*, pages 4681–4690, 2017.
  - [43] Junyong Lee, Sungkil Lee, Sunghyun Cho, and Seungyong Lee. Deep defocus map estimation using domain adaptation. In *Proceedings of the IEEE Conference on Computer Vision and Pattern Recognition (CVPR)*, pages 12222–12230, 2019.
  - [44] Junyong Lee, Hyeonseok Son, Jaesung Rim, Sunghyun Cho, and Seungyong Lee. Iterative filter adaptive network for single image defocus deblurring. In *Proceedings of the IEEE Conference on Computer Vision and Pattern Recognition (CVPR)*, pages 2034–2042, 2021.
  - [45] Xia Li, Jianlong Wu, Zhouchen Lin, Hong Liu, and Hongbin Zha. Recurrent squeeze-and-excitation context aggregation net for single image deraining. In *Proceedings of the*

- European Conference on Computer Vision (ECCV)*, pages 254–269, 2018.
- [46] Yawei Li, Kai Zhang, Jiezhang Cao, Radu Timofte, and Luc Van Gool. Localvit: Bringing locality to vision transformers. *arXiv preprint arXiv:2104.05707*, 2021.
  - [47] Jingyun Liang, Jiezhang Cao, Guolei Sun, Kai Zhang, Luc Van Gool, and Radu Timofte. Swinir: Image restoration using swin transformer. In *Proceedings of the IEEE International Conference on Computer Vision (ICCV)*, pages 1833–1844, 2021.
  - [48] Ding Liu, Bihan Wen, Yuchen Fan, Chen Change Loy, and Thomas S Huang. Non-local recurrent network for image restoration. In *Proceedings of the Advances in Neural information processing systems (NeurIPS)*, 2018.
  - [49] Ding Liu, Bihan Wen, Yuchen Fan, Chen Change Loy, and Thomas S Huang. Non-local recurrent network for image restoration. In *Proceedings of the Advances in Neural information processing systems (NeurIPS)*, 2018.
  - [50] Pengju Liu, Hongzhi Zhang, Kai Zhang, Liang Lin, and Wangmeng Zuo. Multi-level wavelet-cnn for image restoration. In *Proceedings of the IEEE Conference on Computer Vision and Pattern Recognition Workshops (CVPRW)*, pages 773–782, 2018.
  - [51] Ze Liu, Yutong Lin, Yue Cao, Han Hu, Yixuan Wei, Zheng Zhang, Stephen Lin, and Baining Guo. Swin transformer: Hierarchical vision transformer using shifted windows. In *Proceedings of the IEEE International Conference on Computer Vision (ICCV)*, pages 10012–10022, 2021.
  - [52] Ilya Loshchilov and Frank Hutter. Sgdr: Stochastic gradient descent with warm restarts. In *Proceedings of the International Conference on Learning Representations (ICLR)*, 2017.
  - [53] Kede Ma, Zhengfang Duanmu, Qingbo Wu, Zhou Wang, Hongwei Yong, Hongliang Li, and Lei Zhang. Waterloo exploration database: New challenges for image quality assessment models. *IEEE Transactions on Image Processing (TIP)*, 26(2):1004–1016, 2016.
  - [54] David Martin, Charless Fowlkes, Doron Tal, and Jitendra Malik. A database of human segmented natural images and its application to evaluating segmentation algorithms and measuring ecological statistics. In *Proceedings of the IEEE International Conference on Computer Vision (ICCV)*, pages 416–423, 2001.
  - [55] Chong Mou, Jian Zhang, and Zhuoyuan Wu. Dynamic attentive graph learning for image restoration. In *Proceedings of the IEEE International Conference on Computer Vision (ICCV)*, pages 4328–4337, 2021.
  - [56] Seungjun Nah, Tae Hyun Kim, and Kyoung Mu Lee. Deep multi-scale convolutional neural network for dynamic scene deblurring. In *Proceedings of the IEEE Conference on Computer Vision and Pattern Recognition (CVPR)*, pages 3883–3891, 2017.
  - [57] Ben Niu, Weilei Wen, Wenqi Ren, Xiangde Zhang, Lianping Yang, Shuzhen Wang, Kaihao Zhang, Xiaochun Cao, and Haifeng Shen. Single image super-resolution via a holistic attention network. In *Proceedings of the European Conference on Computer Vision (ECCV)*, pages 191–207. Springer, 2020.
  - [58] Dongwon Park, Dong Un Kang, Jisoo Kim, and Se Young Chun. Multi-temporal recurrent neural networks for progressive non-uniform single image deblurring with incremental temporal training. In *Proceedings of the European Conference on Computer Vision (ECCV)*, pages 327–343, 2020.
  - [59] Yali Peng, Lu Zhang, Shigang Liu, Xiaojun Wu, Yu Zhang, and Xili Wang. Dilated residual networks with symmetric skip connection for image denoising. *Neurocomputing*, 345:67–76, 2019.
  - [60] Tobias Plotz and Stefan Roth. Benchmarking denoising algorithms with real photographs. In *Proceedings of the IEEE Conference on Computer Vision and Pattern Recognition (CVPR)*, pages 1586–1595, 2017.
  - [61] Kuldeep Purohit, Maitreya Suin, AN Rajagopalan, and Vishnu Naresh Boddeti. Spatially-adaptive image restoration using distortion-guided networks. In *Proceedings of the IEEE International Conference on Computer Vision (ICCV)*, pages 2309–2319, 2021.
  - [62] Alec Radford, Karthik Narasimhan, Tim Salimans, Ilya Sutskever, et al. Improving language understanding by generative pre-training. *OpenAI*, 2018.
  - [63] Alec Radford, Jeffrey Wu, Rewon Child, David Luan, Dario Amodei, Ilya Sutskever, et al. Language models are unsupervised multitask learners. *OpenAI*, 2019.
  - [64] Chao Ren, Xiaohai He, Chuncheng Wang, and Zhibo Zhao. Adaptive consistency prior based deep network for image denoising. In *Proceedings of the IEEE Conference on Computer Vision and Pattern Recognition (CVPR)*, pages 8596–8606, 2021.
  - [65] Dongwei Ren, Wangmeng Zuo, Qinghua Hu, Pengfei Zhu, and Deyu Meng. Progressive image deraining networks: A better and simpler baseline. In *Proceedings of the IEEE Conference on Computer Vision and Pattern Recognition (CVPR)*, pages 3937–3946, 2019.
  - [66] Jaesung Rim, Haeyun Lee, Jucheol Won, and Sunghyun Cho. Real-world blur dataset for learning and benchmarking deblurring algorithms. In *Proceedings of the European Conference on Computer Vision (ECCV)*, pages 184–201. Springer, 2020.
  - [67] Olaf Ronneberger, Philipp Fischer, and Thomas Brox. U-net: Convolutional networks for biomedical image segmentation. In *Proceedings of the Medical Image Computing and Computer Assisted Intervention (MICCAI)*, pages 234–241. Springer, 2015.
  - [68] Noam Shazeer. Glu variants improve transformer. *arXiv preprint arXiv:2002.05202*, 2020.
  - [69] Ziyi Shen, Wenguan Wang, Xiankai Lu, Jianbing Shen, Haibin Ling, Tingfa Xu, and Ling Shao. Human-aware motion deblurring. In *Proceedings of the IEEE International Conference on Computer Vision (ICCV)*, pages 5572–5581, 2019.
  - [70] Jianping Shi, Li Xu, and Jiaya Jia. Just noticeable defocus blur detection and estimation. In *Proceedings of the IEEE Conference on Computer Vision and Pattern Recognition (CVPR)*, pages 657–665, 2015.
  - [71] Wenzhe Shi, Jose Caballero, Ferenc Huszár, Johannes Totz, Andrew P Aitken, Rob Bishop, Daniel Rueckert, and Zehan



- Wang. Real-time single image and video super-resolution using an efficient sub-pixel convolutional neural network. In *Proceedings of the IEEE Conference on Computer Vision and Pattern Recognition (CVPR)*, pages 1874–1883, 2016.
- [72] Hyeonseok Son, Junyong Lee, Sunghyun Cho, and Seungyong Lee. Single image defocus deblurring using kernel-sharing parallel atrous convolutions. In *Proceedings of the IEEE International Conference on Computer Vision (ICCV)*, pages 2642–2650, 2021.
- [73] Maitreya Suin, Kuldeep Purohit, and A. N. Rajagopalan. Spatially-attentive patch-hierarchical network for adaptive motion deblurring. In *Proceedings of the IEEE Conference on Computer Vision and Pattern Recognition (CVPR)*, pages 3606–3615, 2020.
- [74] Xin Tao, Hongyun Gao, Xiaoyong Shen, Jue Wang, and Jiaya Jia. Scale-recurrent network for deep image deblurring. In *Proceedings of the IEEE Conference on Computer Vision and Pattern Recognition (CVPR)*, pages 8174–8182, 2018.
- [75] Chunwei Tian, Yong Xu, and Wangmeng Zuo. Image denoising using deep cnn with batch renormalization. *Neural Networks*, 121:461–473, 2020.
- [76] Radu Timofte, Vincent De Smet, and Luc Van Gool. Anchored neighborhood regression for fast example-based super-resolution. In *Proceedings of the IEEE International Conference on Computer Vision (ICCV)*, pages 1920–1927, 2013.
- [77] Zhengzhong Tu, Hossein Talebi, Han Zhang, Feng Yang, Peyman Milanfar, Alan Bovik, and Yinxiao Li. Maxim: Multi-axis mlp for image processing. In *Proceedings of the IEEE Conference on Computer Vision and Pattern Recognition (CVPR)*, pages 5769–5780, 2022.
- [78] Dmitry Ulyanov, Andrea Vedaldi, and Victor Lempitsky. Deep image prior. In *Proceedings of the IEEE Conference on Computer Vision and Pattern Recognition (CVPR)*, pages 9446–9454, 2018.
- [79] Ashish Vaswani, Noam Shazeer, Niki Parmar, Jakob Uszkoreit, Llion Jones, Aidan N Gomez, Łukasz Kaiser, and Illia Polosukhin. Attention is all you need. In *Proceedings of the Advances in Neural information processing systems (NeurIPS)*, 2017.
- [80] Wenhai Wang, Enze Xie, Xiang Li, Deng-Ping Fan, Kaitao Song, Ding Liang, Tong Lu, Ping Luo, and Ling Shao. Pyramid vision transformer: A versatile backbone for dense prediction without convolutions. In *Proceedings of the IEEE International Conference on Computer Vision (ICCV)*, pages 568–578, 2021.
- [81] Xiaolong Wang, Ross Girshick, Abhinav Gupta, and Kaiming He. Non-local neural networks. In *Proceedings of the IEEE Conference on Computer Vision and Pattern Recognition (CVPR)*, pages 7794–7803, 2018.
- [82] Xintao Wang, Ke Yu, Shixiang Wu, Jinjin Gu, Yihao Liu, Chao Dong, Yu Qiao, and Chen Change Loy. Esrgan: Enhanced super-resolution generative adversarial networks. In *Proceedings of the European Conference on Computer Vision Workshops (ECCVW)*, pages 0–0, 2018.
- [83] Zhendong Wang, Xiaodong Cun, Jianmin Bao, Wengang Zhou, Jianzhuang Liu, and Houqiang Li. Uformer: A general u-shaped transformer for image restoration. In *Proceedings of the IEEE Conference on Computer Vision and Pattern Recognition (CVPR)*, pages 17683–17693, 2022.
- [84] Wei Wei, Deyu Meng, Qian Zhao, Zongben Xu, and Ying Wu. Semi-supervised transfer learning for image rain removal. In *Proceedings of the IEEE Conference on Computer Vision and Pattern Recognition (CVPR)*, pages 3877–3886, 2019.
- [85] Zhihao Xia and Ayan Chakrabarti. Identifying recurring patterns with deep neural networks for natural image denoising. In *Proceedings of the IEEE Winter Conference on Applications of Computer Vision (WACV)*, pages 2426–2434, 2020.
- [86] Zhenda Xie, Zheng Zhang, Yue Cao, Yutong Lin, Jianmin Bao, Zhuliang Yao, Qi Dai, and Han Hu. Simmim: A simple framework for masked image modeling. In *Proceedings of the IEEE Conference on Computer Vision and Pattern Recognition (CVPR)*, pages 9653–9663, 2022.
- [87] Li Xu, Shicheng Zheng, and Jiaya Jia. Unnatural l0 sparse representation for natural image deblurring. In *Proceedings of the IEEE Conference on Computer Vision and Pattern Recognition (CVPR)*, pages 1107–1114, 2013.
- [88] Wenhan Yang, Robby T Tan, Jiashi Feng, Jiaying Liu, Zongming Guo, and Shuicheng Yan. Deep joint rain detection and removal from a single image. In *Proceedings of the IEEE Conference on Computer Vision and Pattern Recognition (CVPR)*, pages 1357–1366, 2017.
- [89] Rajeev Yasarla and Vishal M Patel. Uncertainty guided multi-scale residual learning-using a cycle spinning cnn for single image de-raining. In *Proceedings of the IEEE Conference on Computer Vision and Pattern Recognition (CVPR)*, pages 8405–8414, 2019.
- [90] Zongsheng Yue, Hongwei Yong, Qian Zhao, Deyu Meng, and Lei Zhang. Variational denoising network: Toward blind noise modeling and removal. In *Proceedings of the Advances in Neural information processing systems (NeurIPS)*, 2019.
- [91] Zongsheng Yue, Qian Zhao, Lei Zhang, and Deyu Meng. Dual adversarial network: Toward real-world noise removal and noise generation. In *Proceedings of the European Conference on Computer Vision (ECCV)*, pages 41–58, 2020.
- [92] Syed Waqas Zamir, Aditya Arora, Salman Khan, Munawar Hayat, Fahad Shahbaz Khan, and Ming-Hsuan Yang. Restormer: Efficient transformer for high-resolution image restoration. In *Proceedings of the IEEE Conference on Computer Vision and Pattern Recognition (CVPR)*, pages 5728–5739, 2022.
- [93] Syed Waqas Zamir, Aditya Arora, Salman Khan, Munawar Hayat, Fahad Shahbaz Khan, Ming-Hsuan Yang, and Ling Shao. CycleISP: Real image restoration via improved data synthesis. In *Proceedings of the IEEE Conference on Computer Vision and Pattern Recognition (CVPR)*, pages 2696–2705, 2020.
- [94] Syed Waqas Zamir, Aditya Arora, Salman Khan, Munawar Hayat, Fahad Shahbaz Khan, Ming-Hsuan Yang, and Ling Shao. Learning enriched features for real image restoration and enhancement. In *Proceedings of the European Conference on Computer Vision (ECCV)*, pages 492–511, 2020.

- [95] Syed Waqas Zamir, Aditya Arora, Salman Khan, Munawar Hayat, Fahad Shahbaz Khan, Ming-Hsuan Yang, and Ling Shao. Multi-stage progressive image restoration. In *Proceedings of the IEEE Conference on Computer Vision and Pattern Recognition (CVPR)*, pages 14821–14831, 2021.
- [96] Hongyi Zhang, Moustapha Cisse, Yann N Dauphin, and David Lopez-Paz. mixup: Beyond empirical risk minimization. *arXiv preprint arXiv:1710.09412*, 2017.
- [97] Hongguang Zhang, Yuchao Dai, Hongdong Li, and Piotr Koniusz. Deep stacked hierarchical multi-patch network for image deblurring. In *Proceedings of the IEEE Conference on Computer Vision and Pattern Recognition (CVPR)*, pages 5978–5986, 2019.
- [98] He Zhang and Vishal M Patel. Density-aware single image de-raining using a multi-stream dense network. In *Proceedings of the IEEE conference on computer vision and pattern recognition (CVPR)*, pages 695–704, 2018.
- [99] He Zhang, Vishwanath Sindagi, and Vishal M Patel. Image de-raining using a conditional generative adversarial network. *IEEE Transactions on Circuits and Systems for Video Technology (TCSVT)*, 2019.
- [100] Jiawei Zhang, Jinshan Pan, Jimmy Ren, Yibing Song, Linchao Bao, Rynson WH Lau, and Ming-Hsuan Yang. Dynamic scene deblurring using spatially variant recurrent neural networks. In *Proceedings of the IEEE Conference on Computer Vision and Pattern Recognition (CVPR)*, pages 2521–2529, 2018.
- [101] Kai Zhang, Yawei Li, Wangmeng Zuo, Lei Zhang, Luc Van Gool, and Radu Timofte. Plug-and-play image restoration with deep denoiser prior. *IEEE Transactions on Pattern Analysis and Machine Intelligence (TPAMI)*, 44(10):6360–6376, 2021.
- [102] Kaihao Zhang, Wenhan Luo, Yiran Zhong, Lin Ma, Bjorn Stenger, Wei Liu, and Hongdong Li. Deblurring by realistic blurring. In *Proceedings of the IEEE Conference on Computer Vision and Pattern Recognition (CVPR)*, pages 2737–2746, 2020.
- [103] Kai Zhang, Wangmeng Zuo, Yunjin Chen, Deyu Meng, and Lei Zhang. Beyond a gaussian denoiser: Residual learning of deep cnn for image denoising. *IEEE Transactions on Image Processing (TIP)*, 26(7):3142–3155, 2017.
- [104] Kai Zhang, Wangmeng Zuo, Shuhang Gu, and Lei Zhang. Learning deep cnn denoiser prior for image restoration. In *Proceedings of the IEEE Conference on Computer Vision and Pattern Recognition (CVPR)*, pages 3929–3938, 2017.
- [105] Kai Zhang, Wangmeng Zuo, and Lei Zhang. Ffdnet: Toward a fast and flexible solution for cnn-based image denoising. *IEEE Transactions on Image Processing (TIP)*, 27(9):4608–4622, 2018.
- [106] Lei Zhang, Xiaolin Wu, Antoni Buades, and Xin Li. Color demosaicking by local directional interpolation and nonlocal adaptive thresholding. *Journal of Electronic imaging*, 20(2):023016–023016, 2011.
- [107] Yulun Zhang, Kunpeng Li, Kai Li, Lichen Wang, Bineng Zhong, and Yun Fu. Image super-resolution using very deep residual channel attention networks. In *Proceedings of the European Conference on Computer Vision (ECCV)*, pages 286–301, 2018.
- [108] Yulun Zhang, Kunpeng Li, Kai Li, Bineng Zhong, and Yun Fu. Residual non-local attention networks for image restoration. In *Proceedings of the International Conference on Learning Representations (ICLR)*, 2019.
- [109] Yulun Zhang, Yapeng Tian, Yu Kong, Bineng Zhong, and Yun Fu. Residual dense network for image restoration. *IEEE Transactions on Pattern Analysis and Machine Intelligence (TPAMI)*, 43(7):2480–2495, 2020.
- [110] Jinghao Zhou, Chen Wei, Huiyu Wang, Wei Shen, Cihang Xie, Alan Yuille, and Tao Kong. ibot: Image bert pre-training with online tokenizer. In *Proceedings of the International Conference on Learning Representations (ICLR)*, 2022.